First archeomagnetic data from Kenya and Chad: Analysis of iron furnaces from Mount Kenya and Guéra Massif

Brina Madingou Tchibinda, Gwenaël Hervé, Mireille M. Perrin, Freda M'Mbogori, Djimet Guemona, Pierre-Etienne Mathé, Pierre Rochette, David Williamson, Vincent Mourre, Caroline Robion-Brunner

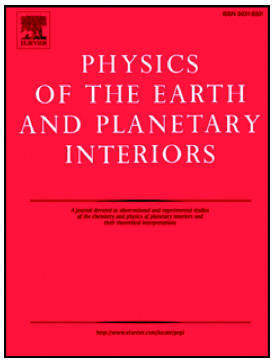

First archeomagnetic data from Kenya and Chad: Analysis of iron furnaces from Mount Kenya and Guéra Massif

Brina Tchibinda Madingou, Gwenaël Hervé, Mireille Perrin, Freda M'Mbogori, Djimet Guemona, Pierre-Etienne Mathé, Pierre Rochette, David Williamson, Vincent Mourre, Caroline Robion-Brunner

PII: S0031-9201(20)30152-7

DOI: https://doi.org/10.1016/j.pepi.2020.106588

Reference: PEPI 106588

To appear in: *Physics of the Earth and Planetary Interiors*

Received date: 19 May 2020

Revised date: 16 September 2020

Accepted date: 22 September 2020

Please cite this article as: B.T. Madingou, G. Hervé, M. Perrin, et al., First archeomagnetic data from Kenya and Chad: Analysis of iron furnaces from Mount Kenya and Guéra Massif, *Physics of the Earth and Planetary Interiors* (2018), https://doi.org/10.1016/j.pepi.2020.106588

First archeomagnetic data from Kenya and Chad: analysis of iron furnaces from Mount Kenya and Guéra Massif

Brina Tchibinda Madingou[1,*], Gwenaël Hervé[2,3], Mireille Perrin[1], Freda M'Mbogori[4], Djimet Guemona[6], Pierre-Etienne Mathé[1], Pierre Rochette[1], David Williamson[5], Vincent Mourre[6], Caroline Robion-Brunner[6]

[1]Aix Marseille Univ, CNRS, IRD, INRAE, Coll France, CEREGE, Aix-en-Provence, France

[2]Univ. Bordeaux Montaigne, CNRS, IRAMAT-CRP2A, UMR 5060, 33607 Pessac, France.

[3]Univ. Rennes 1, CNRS, Géosciences Rennes, UMR 6118, 35000 Rennes, France.

[4]British Institute in Eastern Africa, Nairobi, Kenya.

[5]IRD, ICRAF, Nairobi, Kenya.

[6]Univ. Toulouse 2 le Mirail, CNRS, TRACES, UMR 5608, 31058 Toulouse, France.

Corresponding author: tchibinda@cerege.fr

Keywords: archeomagnetism, secular variation, archeointensity, Africa, iron metallurgy

Abstract

The variation of the Earth's magnetic field over the last millennia is poorly known in Africa, especially in Sub-Saharan Africa that represents less than 1% of the global archeomagnetic dataset. Fourteen iron furnaces from Kenya and Chad have been studied here for archeomagnetic purposes. These structures were dated by ^{14}C from the 14th century in Kenya and from the 18-19th centuries in Chad. Samples, oriented with the plaster cap technique, have been subjected to thermal and alternating field demagnetization, rock magnetic analysis and paleointensity experiment, with the classical Thellier-Thellier technique corrected for anisotropy and cooling rate effects. New directional data (5 from Kenya and 10 from Chad) and one new paleointensity estimate from Kenya (43.5 ± 1.8 µT) were obtained. The Kenyan declinations are in good agreement with the geomagnetic global models, but the inclinations are lower and the intensity higher than predicted. For Chad, the new results prove the efficiency of the archeomagnetic dating, with a precision that is better than radiocarbon for the 18-19th centuries.

1. Introduction

Precise knowledge of the Earth's magnetic field through time is necessary to understand the geodynamo evolution. Direct observations of the geomagnetic field are provided by satellites and ground-based measurements for the last 500 years for declination, 400 years for inclination and since the 1830s for intensity. Using these direct data together with historic data from navigators, a global model gufm1 was calculated for the period 1590-1990 by spherical harmonic analysis of the geomagnetic field (Jackson et al., 2000). This model is nevertheless not well constrained in intensity before 1840. It is therefore needed to

extend knowledge of the Earth's magnetic field, and especially of its secular variation, further back in time and this can be done using either volcanic rocks or baked archeological artefacts that record the local direction and intensity of the geomagnetic field present at the time and place of their last cooling. Sedimentary rocks that also record the direction of the field, can only provide relative paleointensities.

Archeomagnetic data are compiled in databases such as GEOMAGIA50.v3.3 (Brown et al., 2015) and several authors (e.g Constable et al., 2016; Hellio and Gillet, 2018; Arneitz et al., 2019; Campuzano et al., 2019) have developed global spherical harmonic models covering the last 3 to 14 millennia. However, all models are likely to be biased by a strongly uneven geographic distribution, with about 90% of GEOMAGIA50.v3.3 data coming from the Northern hemisphere, and a large majority (~90%) from the mid-latitudes. Africa and South America are the greatest landmasses where we can retrieve data from the equatorial and southern latitudes to address this problem.

In Africa, archeomagnetic and volcanic data, as well as relative data from lake and marine sediments (e.g. Di Chiara, 2019), are rare. Moreover, the large majority of data is concentrated in Northern Africa (e.g. Odah, 1999; Leonhardt et al., 2009; Gómez-Paccard et al., 2012; Casas et al., 2016) and in the Canary Islands (e.g. de Groot et al., 2015; Kissel et al., 2015a, 2015b). Sub-Saharan Africa accounts for only 0.1% of GEOMAGIA50.v3.3 database despite recent additions (e.g. Tanguy et al., 2011 ; Mitra et al., 2013 ; Donadini et al., 2015; Tarduno et al., 2015; Kapper et al., 2017, 2020).

Sub-Saharan Africa is also crucial to understand one of the most remarkable features of the modern geomagnetic field: the South Atlantic Anomaly (SAA). The SAA, currently located in Southern Brazil, is characterized by intensity about 30% weaker at the surface of the globe than if the field was purely dipolar (Thébault et al., 2015). It is generally assumed that the SAA is related to reversed flux patches at the surface of the outer core (e.g. Terra-

Nova et al., 2017). Direct measurements of the geomagnetic field show that since 1840 the SAA intensity minimum drifted to the southwest, about 4500 km at the Earth's surface, associated to an increase of its extent area (e.g. Hartmann & Pacca, 2009; Pavon-Carrasco & De Santis, 2016). Data from Sub-Saharan Africa are crucial to better constrain the path and amplitude of the SAA beyond this date, and especially to confirm if it appeared in the Indian Ocean (Hellio and Gillet, 2018; Campuzano et al., 2019) or in Southern Africa (Tarduno et al., 2015).

Contrary to what the scarcity of archeomagnetic data suggests, the archeological potential is high in Central and Eastern Africa. For archeomagnetic studies, the most frequent well-preserved baked structures are iron furnaces (e.g. Killick, 2016; Robion-Brunner, 2018). In the current state of knowledge, the oldest sites clearly associated to iron metallurgy in Central and Eastern Africa are dated to the first half of the first millennium BCE. This pyrotechnology might even have emerged earlier in the modern Central African Republic at the end of the third millennium BCE (Alpern, 2005; Zangato and Holl, 2010). In this paper, we present archeomagnetic results of iron furnaces dated to the last six centuries in the Mbeere region in Kenya and in the Guéra Massif in Chad (Figure 1a).

2. Archeological setting and sampling

All furnaces were sampled with the plaster cap method (Figures 1b and 1c). Blocks were levelled horizontally with a bubble level and oriented using a magnetic and eventually a sun compass. Between three and six large blocks were collected per furnace. In the laboratory, the blocks were cut into cubic specimens, 2 cm in side, after consolidation in sodium silicate. Two blocks from Kenya and six from Chad could not be used for directional analysis because

their orientation was not precise enough. This is was due either to a damaged plaster cap during transport or to the fragile nature of the samples.

2.1 Mbeere region, Central Kenya

The Kamuturi 1 archeological site (0°25'53" S, 37°47'3" E) that we sampled is located in the Ishiara district of the Mbeere region, close to Mount Kenya (Figure 1a). The site, located at the bottom of a small hill, is assumed to cover an area of 25,000 m^2, based on the extent of visible surface materials. Excavations by F. M'Mbogori between 2015 and 2016 revealed *in situ* furnaces on the eastern side of the site, with several fragments of slag and tuyere pieces in between. To the west of the furnaces, iron working materials are found isolated, more fragmented and in association with daily use objects such as pottery, beads, cowry shells, and metallic artefacts.

All furnaces excavated at Kamuturi 1 site were described as bowl furnaces, made using irregular bricks of clay with maximum length of 15 cm and thickness of 1-4 cm (M'Mbogori et al., in preparation). As some of the best-preserved furnaces were removed for display in a museum, we could only sampled three of the remaining furnaces. Furnace 1 (KAM1-1 in our nomenclature) is the largest with a maximum diameter of 80 cm and a minimum diameter (at bottom) of 42 cm (Figure 1b). The depth from the bottom to the uppermost edge measured 85 cm but bricks scattered on the surface suggest that the furnace stood taller above the ground than the excavated remains. Furnaces 2 and 3 (KAM1-2 and KAM1-3 in our nomenclature), partially excavated, have similar morphology, brick sizes and shapes but they are smaller in size. These differences highlight the complexity of the smelting technologies in use (Iles and Lane, 2015; Iles and Torres, 2009) and it can be noted that the morphology of the excavated furnaces differs from the ethnographic furnaces as described by

Brown (1995). M'Mbogori (2013) points out that the smelters of Kamuturi 1 may have affinities with past communities who lived in this region before the arrival of Bantu groups.

In order to spot additional furnaces, magnetic mapping was done in the area. It is a convenient technique for archeological prospection since buried magnetic objects generate, by contrast with the substratum, a magnetic anomaly. Several EW transects were carried out every 50 cm covering a survey area of 37 m by 20 m around the Kamuturi 1 site. The maps of anomaly gradients (Figures S1a and S1b in the supplementary material) show heterogeneous zones with localized and intense anomalies (maybe related to the slags and the tuyeres), superimposed on a background signal with weaker anomalies and greater wavelength (maybe due to vegetation and soil thickness). The interpretation of these maps is also complicated by previous excavations and by a substratum made of red clay that has an induced magnetization on the same order of magnitude as the furnaces. However, one furnace (KAM1-4) is clearly indicated by an association of positive and negative anomalies, characterizing a magnetic dipole that is remanent since it is not aligned with the local geomagnetic field (Figure S1b). This furnace, comparable in size to KAM1-2, was sampled. After filtering of the lower probe map, the presence of other potential furnaces is suggested (shaded areas in Figure S1c).

Three to six blocks were collected per structure for a total of 17 blocks, a fairly low number compared to other archeomagnetic studies but that could not be enhanced due to preservation constraints. Sampling was also limited by suspicions of post-heating movements due to the surrounding vegetation in some part of the furnaces. The colour of the baked clay used for the walls of the furnaces varies from grey to dark-brown and more reddish parts but without clear relationships with the temperature gradient.

KAM1-1 and KAM1-2 furnaces were dated by radiocarbon on charcoals found in their filling (M'Mbogori et al., in preparation). As the site is located at the equator, the calibration process can be performed using either IntCal13 (Reimer et al., 2013) or SHCal13 (Hogg et al.,

2013) curves, which were designed for the Northern and the Southern hemispheres respectively. The two probability density functions that can be obtained have different shapes and therefore provide slightly different time intervals at 95% of confidence (see Figure S2 in the supplementary material). For example, in the case of KAM1-1, IntCal13 provides two time-intervals of [1452-1528] and [1543-1634] cal CE, while SHCal provides only one [1483-1641] cal CE. In order to cover the two possibilities, the dating of KAM1-1 and KAM1-2 furnaces was cautiously fixed between 1450 and 1650 CE and, considering the usually short use of this type of metallurgical sites in this area (low quantity of scoriae and low number of furnaces per site), we assumed that KAM1-3 and KAM1-4 furnaces are dated from the same period.

2.2 Guéra Massif, central Chad

The Guéra Massif, mainly composed of granites (Shellnutt et al., 2017), is located in south-central Chad. An archeological survey was carried out by Vincent Mourre and Djimet Guémona in the area near Mongo, the main town of the region. One of their main objectives was to locate iron smelting sites, to better constrain the history of this technology in the region. Information collected among the local population place the development of steel industry in the Guéra Massif during the "abasia" period that started between 1611 and 1635 CE and ended around 1909 CE. They also indicate that the local production of iron has been abandoned at the time of the establishment of the French colonial administration in 1908. Three main smelting sites with furnaces have been identified.

Bankakotch site (12°11'01.1''N; 18°49'17.6''E) is located to the south-east of the Abu Telfane chain. It is one of the largest iron sites in the Migami district with a high quantity of scoriae and tuyeres. The three excavated furnaces (BANK1, BANK2 and BANK3) are circular in shape with a diameter between 35 and 58 cm and wall thicknesses between 6 and 12 cm.

Bogrom site (12°09'29.4'N; 18°25'50.2''E) is in the Bitkine district, about 30 km west of Mongo. The four furnaces that were uncovered are conical in shape, with a diameter of about 40 cm and walls about 6 cm thick (Figure 1c). Four furnaces (BOG1, BOG2, BOG3 and BOG4) were sampled.

Djogolo site (12°12'22.4''N; 18°47'55.2''E) is close to Bankakotch site about 12 km east of Mongo. The furnaces here are more semi-circular than those of Bankakotch and Bogrom, with a long axis around 40 cm and a thin wall thickness around 4 cm. Three furnaces (DJO1, DJO2 and DJO3) were sampled.

Between 2 and 4 dark-coloured blocks were collected per furnace, for a total of 34 blocks at the three sites.

Only two furnaces from Bankakotch (BANK1 and BANK2) and three from Bogrom (BOG1, BOG2 and BOG4) could be dated per radiocarbon on charcoals found at the base of the structures (filled with charcoal trapped in scoria). All charcoals were first studied by anthracology by Barbara Eichhorn (Goethe-Universität, Frankfurt/Main). Almost all of them belong to *Prosopis Africana*, a common shrub of savannah in Sub-Saharan Africa. AMS dating at Poznan radiocarbon laboratory were preferentially performed on charcoals from twigs, because they are likely not affected by a significant old-wood effect. Calibration was processed with IntCal13 curve (Figure S3 in the supplementary material). Due to a plateau effect on the calibration curve, ^{14}C intervals are very large (between 1650 and 1950 CE, see supplementary material for details). They agree with the proposed archeological age but do not specify it much. We attributed the maximum ^{14}C range (1650-1950 CE) to all others undated furnaces.

3. Magnetic Mineralogy

Rock magnetic experiments were performed, in order to investigate the ferromagnetic mineralogy and its stability to temperature. All experiments were conducted at CEREGE laboratory.

3.1 K/T curves

The susceptibility of the samples was measured through two successive heating-cooling cycles up to medium (350°C) and high (650°C) temperatures using an AGICO Multi-frequency Kappabridge (MFK1-CS3) apparatus. The experiments were done on 30 and 32 powdered specimens of ~200 mg from Kenyan and Chadian furnaces, respectively. The Curie temperature was estimated at the point at which the curvature of the concave part of the heating curve is maximal (e.g. Dunlop and Özdemir, 1997).

In both cases, we observe mainly two characteristic behaviours in the K/T curves. The first behaviour, that represents ~35% of the Kenyan specimen and ~30% of the Chadian specimens, shows a single ferromagnetic phase that corresponds to an almost pure magnetite with Curie temperatures close to 580°C (Figures 2a and 2b). The mostly reversible curves highlight the absence of mineralogical transformation during heating. It is worth noting that for the Kenyan samples, this behaviour is mainly found in the samples that present a reddish colour. The other specimens, grey or dark-brown in colour, present at least another phase besides this almost pure magnetite. This second behaviour, also seen in the Chadian samples, is illustrated in Figures 2c and 2d. The K/T curves present a first phase that seems to be rather stable at least up to 350-400°C, with Curie temperature around 400-500°C. This is probably a titanomagnetite that will transform at higher temperature into magnetite, explaining the increase of susceptibility in the cooling curves.

3.2 Hysteresis parameters

Hysteresis curves up to 0.5 Tesla and backfield curves were performed on eight Kamuturi 1 specimens and eight Chadian specimens of ~ 5 mm diameter using the Micromag Vibrating Sampling magnetometer 2900 (Figure S4 in supplementary material). Hysteresis parameters were calculated after removal of the paramagnetic component: M_s is the saturation magnetization, M_{rs} the saturation remanent magnetization, B_c the coercive force and B_{cr} the remanent coercive force (Table S1 in supplementary material). In Figure 3, the Day diagram (Day, 1977) that presents the remanence ratio M_{rs}/M_s versus the coercivity ratio B_{cr}/B_c can be used to estimate roughly the domain state of magnetite grains (e.g. Dunlop 2002). All the samples that were measured plot in the pseudo single domain (PSD) range, indicating a common occurrence of large grains within our samples.

4. Directional analysis

All magnetic moments were measured with a 2G cryogenic magnetometer. To retrieve the direction of the remanent magnetizations, 100 cubic specimens (38 from Kenya and 62 from Chad) were demagnetized. Stepwise alternating field (AF) demagnetization was made from 3 to 90 mT (every 5 mT up to 50 mT and every 10 mT between 50 and 90 mT), with the AF demagnetizer built in line with the 2G cryogenic magnetometer. Stepwise thermal demagnetization was done in an MMTD80A oven with 14 steps up to 585°C (every 50°C from 100 to 400°C, every 30°C from 400°C to 520°C, every 20°C from 520°C to 560°C and finally 585°C). For Kenya, 20 specimens were AF and 18 thermally demagnetized. AF demagnetization was in average less noisy than thermal treatment (e.g. Figures 4a and 4c and Table S2). This difference was due to temporary experimental problems with our MMTD80A oven, and we therefore favoured AF demagnetization (56 specimens) for the Chadian

samples. However, a few thermal demagnetizations (6 specimens) were done to determine their unblocking temperature spectrum (e.g. Figures 4b). Results were interpreted with the Puffin Plot software (Lurcock and Wilson, 2012). Most of the plots and the calculation of the mean directions by Fisher statistic were done with the PmagPy3.0 software (Tauxe et al., 2016).

Most of the specimens (80% and 75% from Kenya and Chad respectively) present a single component of magnetization (Figures 4a, 4c and 4d), while a secondary component is also observed for the rest of the samples. As this secondary component is usually removed at fairly low fields or temperatures (Figure 4b, 4e and 4f), it is probably of viscous origin. The directions of the characteristic remanent magnetization (ChRM) per demagnetized specimen are listed in Table S2 of the supplementary material, and the equal area plots of Figure S5 (supplementary material) present the distribution of the ChRM directions per furnace (Table 1). Eight specimens with an aberrant orientation were rejected (with more than 30° to their sister specimens). This is probably related to an error in the transfer of orientation to the specimen.

Most furnaces show a good grouping of their ChRM directions, as evidenced by large kappa. For some furnaces, the dispersion is larger, especially in declination, likely because of slight post-heating wall movements due to tree roots (e.g. for KAM1-3) or during the excavations (e.g. KAM1-1). Despite these dispersions at the cooling unit level, the directions are coherent at the site level (Figure 5, Table 1) and therefore were all considered as representative of the ancient geomagnetic field. They are the first archeomagnetic directions ever obtained from Central and Eastern Africa.

5. Archeointensity determination

For archeointensity determination, we used the classical Thellier-Thellier method (Thellier and Thellier, 1959) with 7-12 temperature steps up to 560°C, distributed according to the unblocking temperature range of the specimens. The protocol consists of heating and cooling the specimens twice at each temperature step with a laboratory field (40μT) applied along the +Z and -Z axis of the specimen successively. To assure a better reproducibility of the experiments, we invert the field and not the specimens. Partial thermoremanent magnetization (pTRM) checks are performed every two steps to monitor the mineralogical transformations. All heatings were performed in an ASC TD48-SC oven with a temperature reproducibility within 1°C. The archeointensity results were interpreted using ThellierTool4.0 software (Leonhardt et al., 2004).

A total of 19 oriented cubic specimens (2 cm in side) from Kenya and 41 from Chad were analysed. In the case of Kenyan furnaces, in order to test if the differences in ferromagnetic mineralogy and colour of the blocks play a role on the results, we also prepared 21 non-oriented grey, brown or reddish small chips embedded in non-magnetic plaster.

A paleointensity estimate is considered as reliable only when the Arai plot is linear over a large proportion of the unblocking temperatures and when the orthogonal diagram shows a single component of magnetization in this interval of temperature. Our acceptance criteria are a quality factor *q* higher than 5 and a paleointensity error lower than 10%. We also consider the consistency within a given furnace and fix an upper limit of ±10% for the standard deviation on the average value.

Only three specimens from one Kenyan furnace (KAM1-1) meet our acceptance criteria (Table 2). KAM1-1.1A11 and KAM1-1.1A21 especially provide convincing results (Figure 6a). The paleointensity estimation of KAM1-1.2A11 is of lower quality with a q factor of 7 but is consistent with the two other accepted specimens (Figure 6b).

Five specimens from Chad have rather linear Arai plots but show two components of magnetization in orthogonal plots (Figure 6c). As the sister-specimens that were AF and thermally demagnetized carry only one component of magnetization, this behaviour is likely explained by mineralogical alteration and specimens must be rejected. The two apparent components of magnetization indicate the acquisition of a chemical remanent magnetization during the laboratory experiment that results in the deviation of the direction along the laboratory field direction (+Z). Finally, most other specimens from Kenya and Chad show two slopes or a concave-up shape on their Arai plot associated to a non-linear orthogonal diagram (Figure 6d). This behaviour can be related to the presence of coarse grains (e.g. Levi, 1977), in line with the Day plot (Figure 3). For Kenya, we checked if there was any relationship between the paleointensity results and the ferromagnetic properties or the colour of the samples without clear results.

The archeointensities of the three accepted specimens from KAM1-1 furnace were corrected for the effects of TRM anisotropy and cooling rate with the protocol of Chauvin et al. (2000). The TRM anisotropy tensor was determined at 550°C with six different positions (+X, -X, +Y, -Y, +Z and -Z) of the specimens. The anisotropy correction could not be applied to KAM1-1.2A11, likely altered by mineralogical transformations, but this is not really crucial with an anisotropy effect of 4.5% and 0.8% for the two others specimens.

The cooling rate correction was performed at the same temperature as the anisotropy correction. It consists in the comparison of two pTRMs acquired during a rapid cooling, over one hour (i.e. the duration used in routine during the Thellier-Thellier procedure) and a slow cooling, to better approximate the original cooling of the furnace. Here the duration of the slow cooling was 5 hours due to experimental constraints of our laboratory oven. It may underestimate the initial archeological cooling but this approximation will have a smaller impact on the accuracy of the average archeointensity than the absence of correction (Hervé et

al., 2019). The cooling rate correction factors of the three specimens range between 8 and 11%. The corrected mean archeointensity of KAM1-1 furnace is 43.5 ± 1.8 μT. Even though the success rate of this study is low, we propose the first full vector determination ever published in Eastern Africa.

6. Interpretation

Over the Holocene, the current update of GEOMAGIA50 v3.3 database (Brown et al., 2015) reports 40 archeointensities and 48 archeodirections in Sub-Saharan Africa, to which have been recently added 18 new archeointensities by Kapper et al. (2020). All these data are dated in the last 3 millennia and most were acquired in Western Africa (Mitra et al., 2013 ; Donadini et al., 2015; Kapper et al., 2017, 2020), La Réunion Island (Tanguy et al., 2011) and South Africa (Neukirch et al., 2012; Tarduno et al., 2015). Data are very rare in Central and Eastern Africa near our sites, emphasizing again the impact of our study. In Cameroon, three directions have been published on volcanic lava flows erupted in the 20th century CE (Herrero-Bervera et al., 2004). In Eastern Africa, Skinner et al. (1975) acquired 13 directions on lava flows but only two of them (data named S and T5) are independently dated with precision to the 19th century CE. An intensity data point has also been published for Ethiopia on bricks produced at the beginning of the 17th century CE (Osete et al., 2015).

Regarding this almost absence of neighbouring data, we first focus the discussion on the comparison with the predictions of four recent global models, CALS10k.2 (Constable et al., 2016), COVARCH (Hellio and Gillet, 2018), BIGMUDI4k.1 (Arneitz et al., 2019) and gufm1 (Jackson et al., 2000). The latter is computed only from direct measurements by navigators or in observatories.

6.1 Comparison of our results with global models

Our new Kenyan data are in good agreement with the global models for the declination (Figure 7a). KAM1-3 has a declination that is ~6° lower than the others furnaces, which may indicate that this furnace did not operate at the same period. The average inclinations of the four furnaces are mutually consistent but they are lower than the average prediction of the models (Figure 7b). The better fit in declination than in inclination could be explained by the fact that the direct measurements were recorded by the navigators along the East African coastline since the 16th century for the declination but only after the 18th century for the inclination (Jonkers et al., 2003; Arneitz et al., 2017).

The new archeointensity obtained on KAM1-1 furnace is around 10 µT higher than the Ethiopian data point of Osete et al. (2015), after relocation to Kamuturi 1 (Figure 7c). Despite the fact that there are only two archeointensity data for East Africa, this difference could indicate a fast secular variation of the geomagnetic field strength in this area at the middle of the second millennium CE, not seen in models due to the lack of intensity data in Africa. New data are needed to obtain more robust models.

The average directions of the ten furnaces from Chad are also compared to global models. The declination values cover the whole range of values predicted by the models since 1600 CE (Figure 8a). However, the average inclinations are consistent with the models only in the recent part of their ^{14}C dating (Figure 8b). This large uncertainty of the ^{14}C dating makes our Chadian results not very useful to improve the archeomagnetic database.

6.2 Archeomagnetic dating of Chadian furnaces

Considering the young age of the Chadian furnaces, our results can however be used to better constrain the age of the furnaces. Archeomagnetic dating is performed with the

prediction at the sites of the gufm1 global model using RenDateModel software (Lanos, 2004). The intervals of date at 95% of confidence are calculated on the combination of the two probability density functions (pdfs) obtained with declination and inclination (Figure 8c for BOG1 furnace and Figure S6 in Supplementary material for other furnaces). No results can be obtained for three furnaces (BANK2, BOG3 and DJO3) that have inconsistent declination and inclination pdfs, maybe because of post-heating movements of ovens walls. For other furnaces, dating provides a single interval of date between the mid-19th and the 20th century CE, that is at the end of the "abasia" period (Figure 8d). These recent dates are in very good agreement with oral sources that suggest an abandonment of the local iron production with the establishment of the French colonial administration in 1908. However, the results of BOG2, BOG4 and DJO2 furnaces indicate that the local production could have slightly continued afterwards.

7. Conclusions

Our archeomagnetic study of 4 furnaces from Kenya and 10 from Chad is the first published in these countries. We obtained 14 new directions (4 for Kenya and 10 for Chad) and one intensity from Kenya. This work illustrates the two complementary applications of archeomagnetism: 1) data acquisition for geomagnetic modelling, 2) archeomagnetic dating.

Sub-Saharan Africa is one of the poorest landmasses in archeomagnetic data. Our new Kenyan data, dated between 1450 and 1650 CE, are a new step to address this problem. The current global models are consistent with our data in declination but not in inclination and intensity. Our new data will clearly contribute to improve them in the future, in order to better retrieve the secular variation of the geomagnetic field in Sub-Saharan Africa and to better understand the origin of the present South Atlantic Anomaly.

The Chadian furnaces are more recent than the Kenyan ones and were used to test the potential of archeomagnetic dating in Africa over the last centuries. The use of gufm1 global model appears a powerful dating tool with a precision much better than the one of radiocarbon for this period.

Acknowledgements

This work was supported by the CEREGE laboratory through its 2017 APIC, and by the Programme National de Planétologie (PNP) of CNRS/INSU, co-funded by CNES, through its 2018 program. The fieldwork in Kenya was made possible through the support of National Museums of Kenya/British Institute in East Africa (BIEA), and the IRD-East Africa representation in Nairobi. The fieldwork in Chad was supported by the ArRéLat program funded by the French Ministry of Foreign Affairs, and by CEREGE/IRD (Pierre Rochette). We have a very special thought for Barbara Eichhorn, recently passed away, whose help was extremely precious to select the samples from Chad that could be safely dated by ^{14}C and whom we regret. The manuscript was improved thanks to reviewers' comments.

Author statement

Brina Tchibinda Madingou, Gwenaël Hervé, Mireille Perrin: Fieldwork, laboratory experiments, analysis, and writing. **Pierre-Etienne Mathé:** Magnetic prospection. **Freda M'Mbogori, Djimet Guemona, Pierre Rochette, David Williamson, Vincent Mourre, Caroline Robion-Brunner:** Field work and sampling.

Declaration of interests

☒ The authors declare that they have no known competing financial interests or personal relationships that could have appeared to influence the work reported in this paper.

References

Alpern, S.B., 2005. Did They or Didn't They Invent It? Iron in Sub-Saharan Africa. History in Africa 32, 41–94. https://doi.org/10.1353/hia.2005.0003

Arneitz, P., Leonhardt, R., Schnepp, E., Heilig, B., Mayrhofer, F., Kovacs, P., Hejda, P., Valach, F., Vadasz, G., Hammerl, C., Egli, R., Fabian, K., Kompein, N., 2017. The HISTMAG database: Combining historical, archaeomagnetic and volcanic data. Geophysical Journal International 210, 3, 1347-1359. https://doi.org/10.1093/gji/ggx245

Arneitz, P., Egli, R., Leonhardt, R., Fabian, K., 2019. A Bayesian iterative geomagnetic model with universal data input: Self-consistent spherical harmonic evolution for the geomagnetic field over the last 4000 years. Physics of the Earth and Planetary Interiors 290, 57–75. https://doi.org/10.1016/j.pepi.2019.03.008

Brown, J., 1995. Traditional metalworking in Kenya. *Cambridge Monographs in African Archaeology* No. 38 Oxbow Monograph 44

Brown, M.C., Donadini, F., Nilsson, A., Panovska, S., Frank, U., Korhonen, K., Schuberth, M., Korte, M., Constable, C.G., 2015. GEOMAGIA50.v3: 2. A new paleomagnetic database for lake and marine sediments. Earth, Planets and Space 67. https://doi.org/10.1186/s40623-015-0233-z

Campuzano, S., Gomez-Paccard, M., Pavon-Carrasco, F.J., Osete, M.L., 2019. Emergence and evolution of the South Atlantic Anomaly revealed by the new paleomagnetic reconstruction SHAWQ2k. Earth and Planetary Science Letters 512, 17-26. https://doi.org/10.1016/j.epsl.2019.01.050

Casas, L., Fouzai, B., Prevosti, M., Laridhi-Ouazaa, N., Járrega, R., Baklouti, S., 2016. New Archaeomagnetic Data from Tunisia: Dating of Two Kilns and New

Archaeointensities from Three Ceramic Artifacts. Geoarchaeology 31, 564–576. https://doi.org/10.1002/gea.21576

Chauvin, A., Garcia, Y., Lanos, Ph., Laubenheimer, F., 2000. Paleointensity of the geomagnetic field recovered on archaeomagnetic sites from France. Physics of the Earth and Planetary Interiors 120, 111–136. https://doi.org/10.1016/S0031-9201(00)00148-5

Constable, C., Korte, M., Panovska, S., 2016. Persistent high paleosecular variation activity in southern hemisphere for at least 10 000 years. Earth and Planetary Science Letters 453, 78–86. https://doi.org/10.1016/j.epsl.2016.08.015

Day, R., M. Fuller, and V. A. Schmidt, Hysteresis properties of titanomagnetites: Grain size and composition dependence, Phys. Earth Planet. Inter., 13, 260–267, 1977.

de Groot, L.V., Béguin, A., Kosters, M.E., van Kissingen, E.M., Struijk, E.L.M., Biggin, A.J., Hurst, E.A., Langereis, C.G., Dekkers, M.J., 2015. High paleointensities for the Canary Islands constrain the Levant geomagnetic high. Earth and Planetary Science Letters 419, 154–167. https://doi.org/10.1016/j.epsl.2015.03.020

Di Chiara, A., 2019. Paleo-secular variations of the geomagnetic field in Africa during Holocene: a Review. Geological Society, London, Special Publications SP497-2019–51. https://doi.org/10.1144/SP497-2019-51

Donadini, F., Serneels, V., Kapper, L., El Kateb, A., 2015. Directional changes of the geomagnetic field in West Africa: Insights from the metallurgical site of Korsimoro. Earth and Planetary Science Letters 430, 349–355. https://doi.org/10.1016/j.epsl.2015.08.030

Dunlop, D.J., 2002. Theory and application of the Day plot (M_{rs}/M_s versus H_{cr}/H_c) 1. Theoretical curves and tests using titanomagnetite data. Journal of Geophysical Research 107. https://doi.org/10.1029/2001JB000486

Dunlop, D., Özdemir, Ö, 1997. *Rock Magnetism*, Cambridge University Press, Cambridge.

Gómez-Paccard, M., McIntosh, G., Chauvin, A., Beamud, E., Pavón-Carrasco, F.J., Thiriot, J., 2012. Archaeomagnetic and rock magnetic study of six kilns from North Africa (Tunisia and Morocco). Geophysical Journal International 189, 169–186.

Hartmann, G. A., and Pacca, I. G. (2009). Time evolution of the South Atlantic Magnetic Anomaly. *Ann. Braz. Acad. Sci.* 81, 243–255. doi: 10.1590/S0001-37652009000200010

Hellio, G., Gillet, N., 2018. Time-correlation-based regression of the geomagnetic field from archeological and sediment records. Geophysical Journal International 214, 1585–1607. https://doi.org/10.1093/gji/ggy214

Herrero-Bervera, E., Ubangoh, R., Aka, F.T., Valet, J.-P., 2004. Paleomagnetic and paleosecular variation study of the Mt. Cameroon volcanics (0.0–0.25 Ma), Cameroon, West Africa. Physics of the Earth and Planetary Interiors 147, 171–182. https://doi.org/10.1016/j.pepi.2004.03.014

Hervé, G., Chauvin, A., Lanos, P., Robbette, P., Perrin, M. & Perron d'Arc, M., 2019. Cooling rate effect on thermoremanent magnetization in archaeological baked clays: an experimental study on modern bricks. Geophysical Journal International, 217, 1413-1424.

Hogg, A.G., Hua, Q., Blackwell, P.G., Niu, M., Buck, C.E., Guilderson, T.P., Heaton, T.J., Palmer, J.G., Reimer, P.J., Reimer, R.W., Turney, C.S.M., Zimmerman, S.R.H., 2013. SHCal13 Southern Hemisphere Calibration, 0–50,000 Years cal BP. Radiocarbon 55, 1889–1903. https://doi.org/10.2458/azu_js_rc.55.16783

Iles, L. and Lane, P., 2015. Iron production in second millennium AD pastoralist contexts on the Laikipia plateau, Kenya, Azania Archaeological Research in Africa http://dx.doi.org/10.1080/0067270X.2015.1079379

Iles, L. and Torres, M., 2009. Pastoralist iron production on the Laikipia Plateau, Kenya: wider implications for archaeometallurgical studies Journal of Archaeological Science (36) 2314-234

Jackson, A., Jonkers, A.R., Walker, M.R., 2000. Four centuries of geomagnetic secular variation from historical records. Philosophical Transactions of the Royal Society of London A: Mathematical, Physical and Engineering Sciences 358, 957–990.

Jonkers, A.R.T., 2003. Four centuries of geomagnetic data from historical records. Reviews of Geophysics 41. https://doi.org/10.1029/2002RG000115

Kapper, L., Donadini, F., Serneels, V., Tema, E., Goguitchaichvili, A., Julio Morales, J., 2017. Reconstructing the Geomagnetic Field in West Africa: First Absolute Intensity Results from Burkina Faso. Scientific Reports 7. https://doi.org/10.1038/srep45225

Kapper, L., Serneels, V., Panovska, S., Ruíz, R.C., Hellio, G., Groot, L. de, Goguitchaichvili, A., Morales, J., Ruíz, R.C., 2020. Novel insights on the geomagnetic field in West Africa from a new intensity reference curve (0-2000 AD). Scientific Reports 10. https://doi.org/10.1038/s41598-020-57611-9

Killick, D., 2016. A global perspective on the pyrotechnologies of Sub-Saharan Africa. Azania: Archaeological Research in Africa 51, 62–87. https://doi.org/10.1080/0067270X.2016.1150082

Kissel, C., Laj, C., Rodriguez-Gonzalez, A., Perez-Torrado, F., Carracedo, J.C., Wandres, C., 2015a. Holocene geomagnetic field intensity variations: Contribution from the low latitude Canary Islands site. Earth and Planetary Science Letters 430, 178–190. https://doi.org/10.1016/j.epsl.2015.08.005

Kissel, C., Rodriguez-Gonzalez, A., Laj, C., Perez-Torrado, F., Carracedo, J.C., Wandres, C., Guillou, H., 2015b. Paleosecular variation of the earth magnetic field at the Canary

Islands over the last 15 ka. Earth and Planetary Science Letters 412, 52–60. https://doi.org/10.1016/j.epsl.2014.12.031

Lanos Ph., 2004. Bayesian inference of calibration curves: application to archaeomagnetism. In: Buck C. and Millard A. (Eds.), Tools for Constructing Chronologies: Crossing Disciplinary Boundaries. Lecture Notes in Statistics., 177, 4382, Springer-Verlag, London, U.K.

Leonhardt, R., Heunemann, C., Krása, D., 2004. Analyzing absolute paleointensity determinations: Acceptance criteria and the software ThellierTool4.0. Geochemistry, Geophysics, Geosystems 5. https://doi.org/10.1029/2004GC000807

Leonhardt, R., Saleh, A., Ferk, A., 2009. Archaeomagnetic field intensity during the Roman period at Siwa and Bahryn oasis, Egypt: Implications for the fidelity of Egyptian archaeomagnetic data. Archaeometry 52, 502–516. https://doi.org/10.1111/j.1475-4754.2009.00508.x

Levi, S., 1977. The effect of magnetite particle size on paleointensity determinations of the geomagnetic field. Phys. Earth Planet. Inter. 13:245-259

Lurcock, P.C., Wilson, G.S., 2012. PuffinPlot: A versatile, user-friendly program for paleomagnetic analysis. technical brief. Geochemistry, Geophysics, Geosystems 13. https://doi.org/10.1029/2012GC004098

M'Mbogori F.N., 2013. Late Iron Age technology of Mt. Kenya region: the case study of the Kangai and Kanyua archaeological sites in Mbeere District. In Humphris, J and Rehren T. (eds) *The World of Iron* London, Archtype Publication Ltd, 46-55.

M'Mbogori, F.N., Davies, M.J., in preparation. Revisiting the Bantu migration narrative: a case study from Mt. Kenya region

Mitra, R., Tauxe, L., Keech McIntosh, S., 2013. Two thousand years of archeointensity from West Africa. Earth and Planetary Science Letters 123–133.

Neukirch, L.P., Tarduno, J.A., Huffman, T.N., Watkeys, M.K., Scribner, C.A., Cottrell, R.D., 2012. An archeomagnetic analysis of burnt grain bin floors from ca. 1200 to 1250 AD Iron-Age South Africa. Physics of the Earth and Planetary Interiors 190–191, 71–79. https://doi.org/10.1016/j.pepi.2011.11.004

Odah, H., 1999. Improvement of the secular variation curve of the geomagnetic field in Egypt during the last 6000 years. Earth, planets and space 51, 1325–1329.

Osete, M.L., Catanzariti, G., Chauvin, A., Pavón-Carrasco, F.J., Roperch, P., Fernández, V.M., 2015. First archaeomagnetic field intensity data from Ethiopia, Africa (1615±12AD). Physics of the Earth and Planetary Interiors 242, 24–35. https://doi.org/10.1016/j.pepi.2015.03.003

Pavon-Carrasco, F.J. & De Santis, A., 2016. The South Atlantic Anomaly: The Key for a Possible Geomagnetic Reversal. *Frontiers Earth Sci.*, 4:40. doi: 10.3389/feart.2016.00040

Reimer, P.J., Bard, E., Bayliss, A., Beck, J.W., Blackwell, P.G., Ramsey, C.B., Buck, C.E., Cheng, H., Edwards, R.L., Friedrich, M., Grootes, P.M., Guilderson, T.P., Haflidason, H., Hajdas, I., Hatté, C., Heaton, T.J., Hoffmann, D.L., Hogg, A.G., Hughen, K.A., Kaiser, K.F., Kromer, B., Manning, S.W., Niu, M., Reimer, R.W., Richards, D.A., Scott, E.M., Southon, J.R., Staff, R.A., Turney, C.S.M., 2013. IntCal13 AND Marine13 radiocarbon age calibration curves 0-50,000 years Cal BP. Radiocarbon 55, 4, 1869-1887.

Robion-Brunner, C., 2018. L'Afrique des métaux. In Fauvelle, F.X., *De l'Acacus au Zimbabwe 20000 avant notre ère – XVII^{e} siècle*, Belin, Paris, pp. 520-543.

Shellnutt, J.G., Pham, N.H.T., Denyszyn, S.W., Yeh, M.-W., Lee, T.-Y., 2017. Timing of collisional and post-collisional Pan-African Orogeny silicic magmatism in south-central Chad. Precambrian Research 301, 113-123.

Skinner, N.J., Iles, W., Brock, A., 1975. The recent secular variation of declination and inclination in Kenya. Earth and Planetary Science Letters 25, 338–346. https://doi.org/10.1016/0012-821X(75)90251-4

Tanguy, J.-C., Bachèlery, P., Le Goff, M., 2011. Archeomagnetism of Piton de la Fournaise: Bearing on volcanic activity at La Réunion Island and geomagnetic secular variation in Southern Indian Ocean. Earth Planetary Science Letters 303, 361-368.

Tarduno, J.A., Watkeys, M.K., Huffman, T.N., Cottrell, R.D., Blackman, E.G., Wendt, A., Scribner, C.A., Wagner, C.L., 2015. Antiquity of the South Atlantic Anomaly and evidence for top-down control on the geodynamo. Nature Communications 6. https://doi.org/10.1038/ncomms8865

Tauxe, L., Shaar, R., Jonestrask, L., Swanson-Hysell, N.L., Minnett, R., Koppers, A.A.P., Constable, C.G., Jarboe, N., Gaastra, K., Fairchild, L., 2016. PmagPy: Software package for paleomagnetic data analysis and a bridge to the Magnetics Information Consortium (MagIC) Database. Geochemistry, Geophysics, Geosystems 17, 2450–2463. https://doi.org/10.1002/2016GC006307

Terra-Nova, F., Amit, H., Hartmann, G.A., Trindade, R.I.F., Pinheiro, K.J., 2017. Relating the South Atlantic Anomaly and geomagnetic flux patches. Physics of the Earth and Planetary Interiors 266, 39–53. https://doi.org/10.1016/j.pepi.2017.03.002

Thébault, E., Finlay, C. C., Beggan, C. D., Alken, P., Aubert, J., Barrois, O., Bertrand, F., Bondar, T., Boness, A., Brocco, L., Canet, E., Chambodut, A., Chulliat, A., Coïsson, P., Civet, F., Du, A., Fournier, A., Fratter, I., Gillet, N., Hamilton, B., Hamoudi, M., Hulot, G., Jager, T., Korte, M., Kuang, W., Lalanne, X., Langlais, B., Jager, J.-M., Lesur, V., Lowes, F. J., et al, 2015. International Geomagnetic Reference Field: the twelfth generation. Earth Planets Space 67:79, doi:10.1186/s40623–015–0228–9.

Thellier, E., Thellier, O., 1959. Sur l'intensité du champ magnétique terrestre dans le passé historique et géologique. Annales de Géophysique 15, 285–376.

Zangato, É., Holl, A.F.C., 2010. On the Iron Front: New Evidence from North-Central Africa. Journal of African Archaeology 8, 7–23. https://doi.org/10.3213/1612-1651-10153

Figure 1: Location of the study areas (a) and examples of furnaces sampled at Kamuturi 1 (KAM1-1 furnace) in Kenya (b) and at Bogrom (BOG4 furnace) in Chad (c).

Figure 2: Representative K/T curves from Kenya (a-c) and Chad (b-d). Heating/cooling curves are in red/blue respectively.

Figure 3: Day plot (Day, 1977) of samples from Kenya and Chad.

Figure 4: Orthogonal diagrams, AF demagnetization and thermal demagnetization curves for representative specimens from Kenya (a-c-e) and Chad (b-d-f). On the orthogonal plots, the open/full squares correspond to the vertical/horizontal projections, respectively. The red symbols indicated the demagnetization steps that were selected to estimate the direction of the characteristic remanent magnetization.

Figure 5: Mean directions of characteristic remanent magnetizations by furnace with their α_{95} confidence circles. Open/full circles correspond to negative/positive inclinations.

Figure 6: Arai plots of representative archeointensity results with corresponding orthogonal diagrams. The solid red circles on the Arai diagrams indicate the temperature steps used in the intensity determination. Triangles indicate pTRM-checks. Temperatures are in degrees Celsius. On the orthogonal plots, the open (solid) circles denote the projection on the vertical (horizontal) plane.

Figure 7: Comparison of the Kamuturi 1 data (red triangles) with existing Eastern Africa data and predictions at the site of recent global models. Skinner and al. (1975) directional data (green circles) were relocated to Kamuturi 1 using Virtual Geomagnetic Pole assumption (a,b). Osete and al. (2015) intensity data point (purple square) was relocated via the Virtual Axial Dipole Moment (c).

Figure 8: (a, b) Comparison of the new Chadian data with the predictions of gufm1, CALS10k.2, COV-ARCH and BIGMUDI4k.1 models. Orange circles correspond to Bankakotch site, light green triangles to Bogrom site and dark green stars to Djogolo site. (c) Archeomagnetic dating of BOG 1 furnace using gufm1 model with probability density functions obtained with declination, inclination and their combination.

Table captions

Table 1: Mean directions of the characteristic remanent magnetizations by furnace. Columns from left to right: country name, site name, latitude and longitude of the site, furnace name, number of blocks used/sampled, number of specimens used to calculate the average value over the number of measured specimens, mean declination and mean inclination, Fisher precision parameter, and Fisher 95% confidence circle, archeomagnetic dating of Chad furnace in years CE.

Country	Site	Lat° N	Long° E	Furnace	N/N_0	n/n_0	Dec °	Inc °	kappa	α_{95} °	AM dating
Kenya	Kamuturi 1	-0.431	37.784	KAM1-1	6/6	12/14	1.8	-3.5	61	5.6	
				KAM1-2	3/3	7/10	1.5	0.3	193	4.4	
				KAM1-3	4/5	7/7	355.2	0.5	120	5.5	
				KAM1-4	2/3	7/7	0.6	-2.1	144	5.0	
Chad	Bankakotch	12.184	18.822	BANK1	3/4	6/6	343.2	1.8	51	9.5	1829-1929
				BANK	2/4	3/3	339.	2.8	282	7.4	unreliabl

				2			1				e
				BANK 3	2/3	4/4	349.0	7.6	104	9.1	1827-1950
	Bogrom	12.158	18.431	BOG 1	3/4	5/5	349.2	8.8	268	4.7	1848-1911
				BOG 2	4/4	7/8	359.2	1.5	79	6.8	1938-2000
				BOG 3	3/4	7/7	5.0	7.1	115	5.7	unreliable
				BOG 4	2/2	8/8	355.7	5.7	84	6.1	1907-1996
	Djogolo	12.206	18.799	DJO 1	4/4	8/9	353.2	3.8	37	9.2	1871-1996
				DJO 2	3/3	7/8	353.3	2.9	125	5.4	1902-1984
				DJO 3	2/2	4/4	2.9	5.2	395	4.6	unreliable

Table 2: Summary of accepted archeointensity results. Columns from left to right: furnace name, specimen name, temperature interval used for the intensity calculation, uncorrected intensity, standard deviation on the intensity, NRM fraction, gap factor, quality factor, intensity corrected for cooling rate effect.

Furnace	**Specimen**	**Interval °C**	**F (µT)**	**sd (µT)**	**f**	**g**	**q**	**F_{CR} (µT)**
KAM1-1	1A11	150-500	47.1	0.7	0.6	0.8	31	44.0
	1A21	150-500	46.7	1.1	0.6	0.8	21	41.5
	2A11	150-450	49.0	2.8	0.6	0.7	7	45.1
							Mean	43.5 ± 1.8

Highlights

- Africa's Sub-Saharan data represents less than 1% of the global archaeomagnetic database
- First archeomagnetic study in Kenya (16th century CE) and Chad (18-19th c. CE)
- Fourteen new directions and one new intensity data
- Inconsistency with geomagnetic models in inclination and intensity
- Archaeomagnetic dating more precise than radiocarbon in the 18-19th c. CE

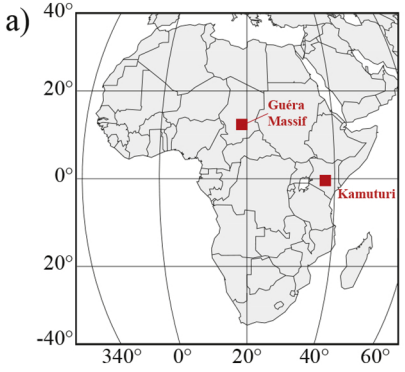

Figure 1

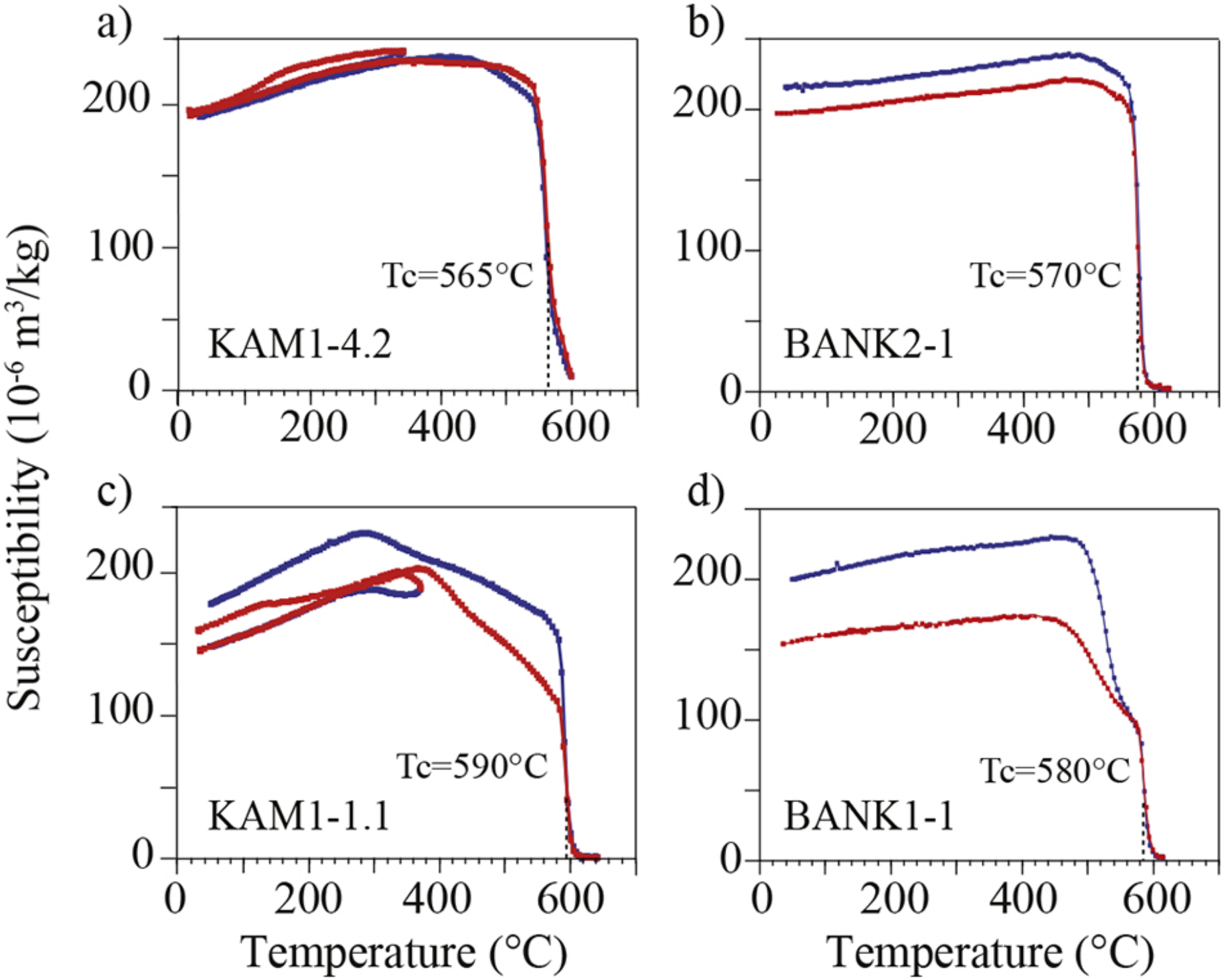
a)
b)
c)
d)
Tc=565°C
KAM1-4.2
Tc=570°C
BANK2-1
Tc=590°C
KAM1-1.1
Tc=580°C
BANK1-1
Susceptibility (10-6 m3/kg)
Temperature (°C)
Temperature (°C)
0
100
200
0
200
400
600

Figure 2

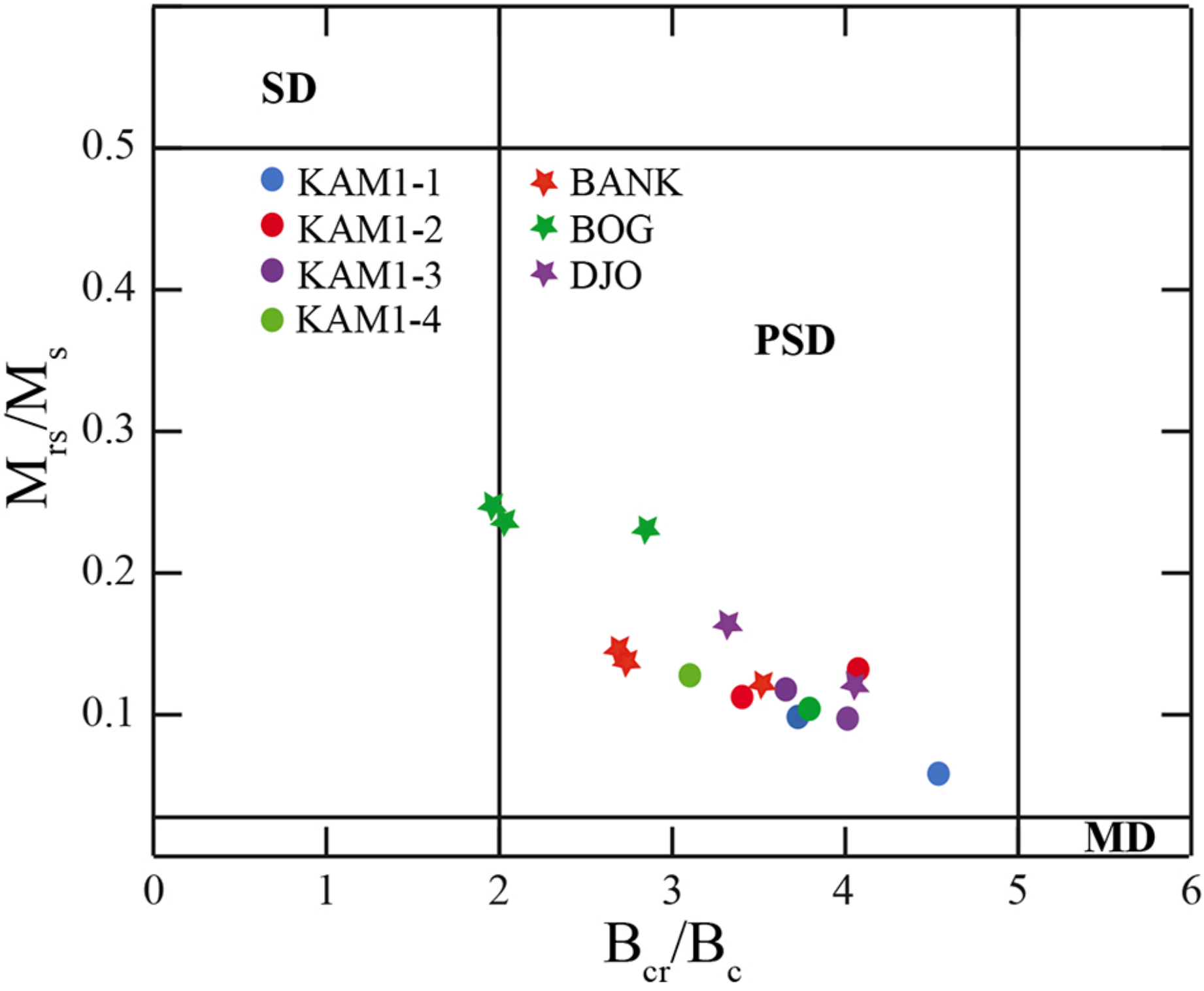
SD
PSD
MD
KAM1-1
KAM1-2
KAM1-3
KAM1-4
BANK
BOG
DJO
0.5
0.4
0.3
0.2
0.1
0
1
2
3
4
5
6
M_{rs}/M_s
B_{cr}/B_c

Figure 3

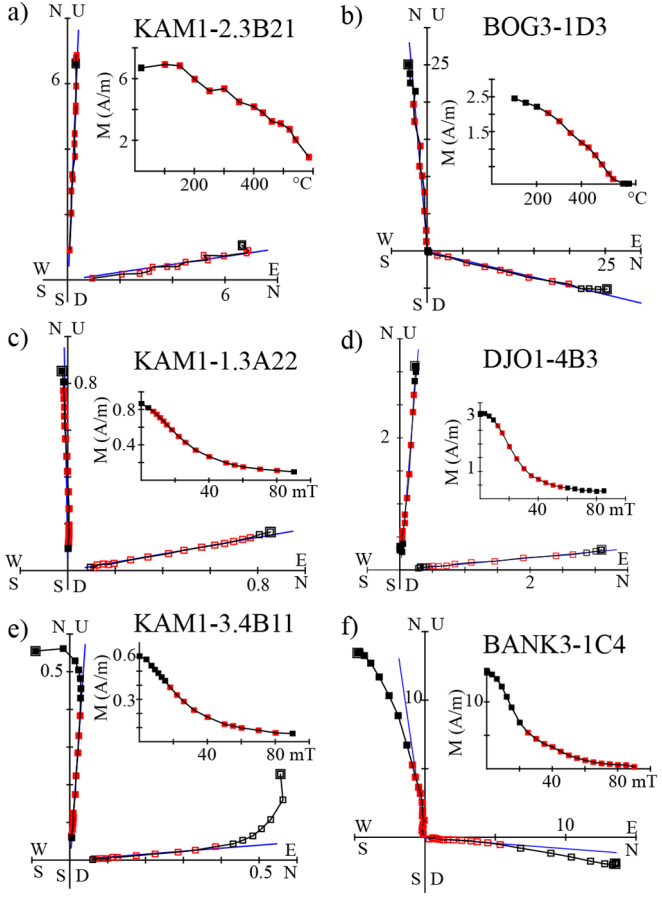
a)
KAM1-2.3B21
N U
6
M (A/m)
6
2
200
400
°C
W
E
S
S D
6
N
b)
BOG3-1D3
N U
25
2.5
1.5
M (A/m)
200
400
°C
W
E
S
25
N
S D
c)
KAM1-1.3A22
N U
0.8
M (A/m)
0.8
0.4
40
80 mT
W
E
S
S D
0.8
N
d)
DJO1-4B3
N U
2
M (A/m)
3
1
40
80 mT
W
E
S
S D
2
N
e)
KAM1-3.4B11
N U
0.5
M (A/m)
0.6
0.3
40
80 mT
W
E
S
S D
0.5
N
f)
BANK3-1C4
N U
10
M (A/m)
10
40
80 mT
W
10
E
S
N
S D

Figure 4

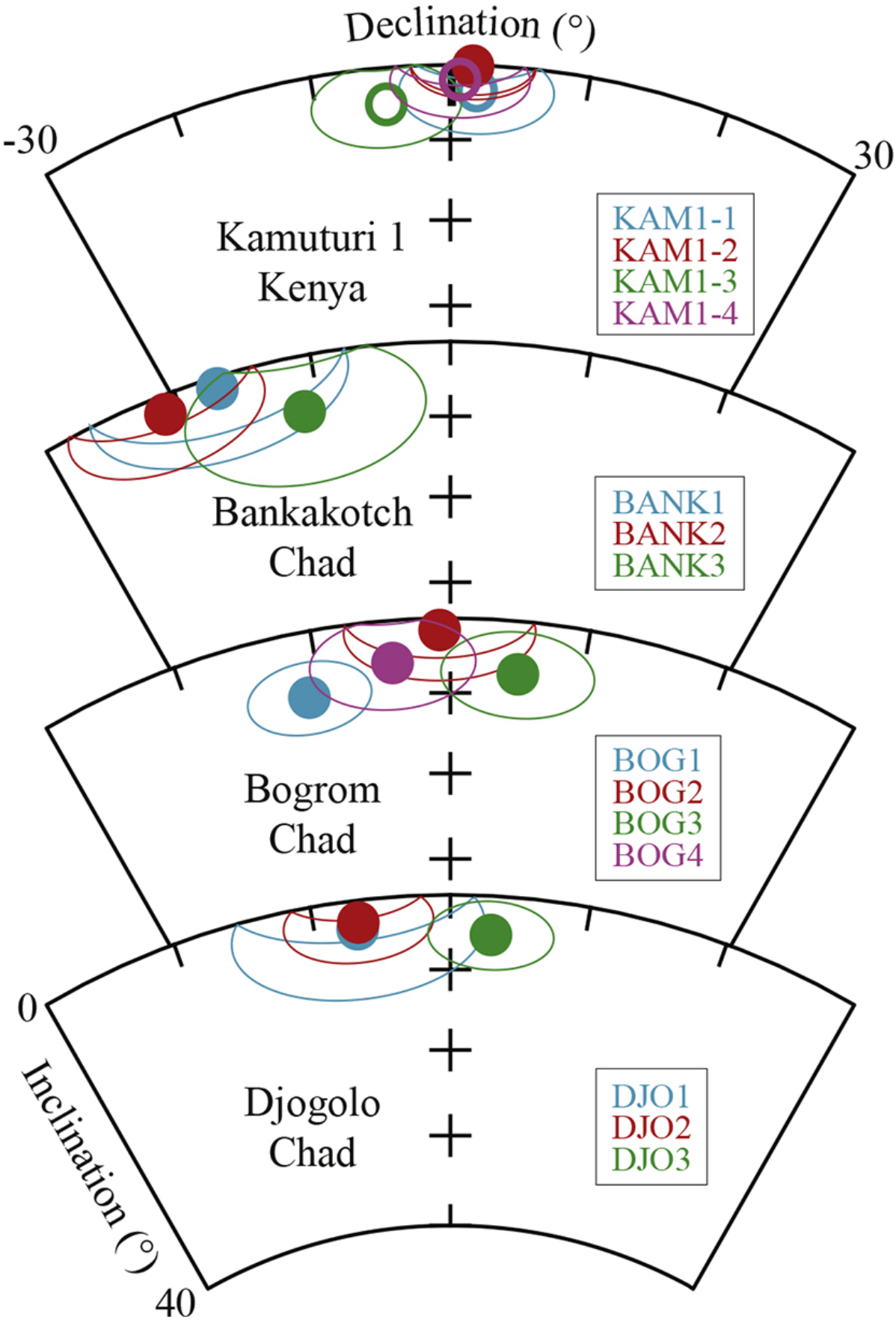
Declination (°)
-30
30
Kamuturi 1
Kenya
KAM1-1
KAM1-2
KAM1-3
KAM1-4
Bankakotch
Chad
BANK1
BANK2
BANK3
Bogrom
Chad
BOG1
BOG2
BOG3
BOG4
Djogolo
Chad
DJO1
DJO2
DJO3
0
Inclination (°)
40

Figure 5

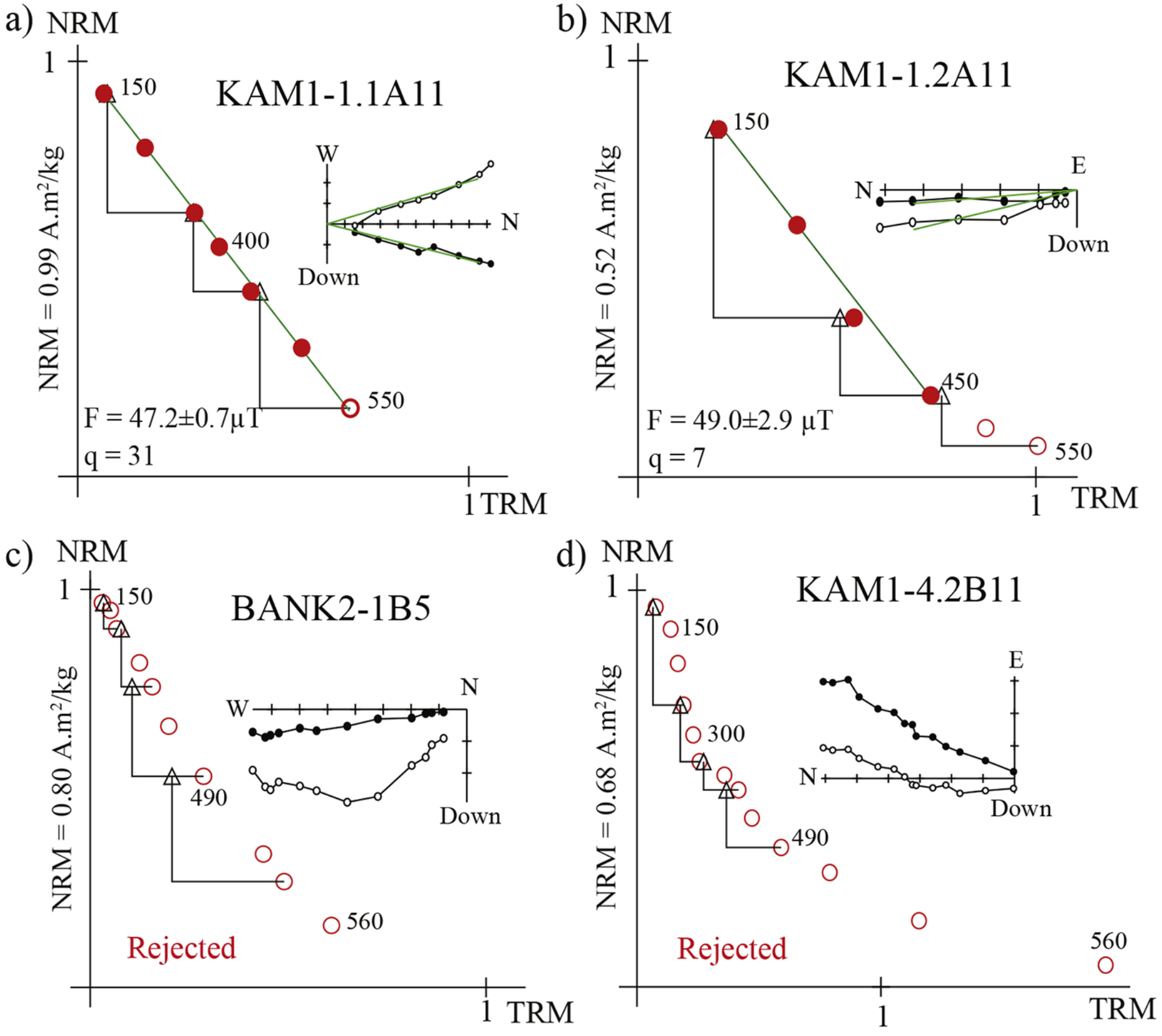
a) NRM
1
KAM1-1.1A11
150
400
550
W
N
Down
NRM = 0.99 A.m²/kg
F = 47.2±0.7μT
q = 31
1 TRM
b) NRM
1
KAM1-1.2A11
150
450
550
E
N
Down
NRM = 0.52 A.m²/kg
F = 49.0±2.9 μT
q = 7
1
TRM
c) NRM
1
BANK2-1B5
150
490
560
W
N
Down
NRM = 0.80 A.m²/kg
Rejected
1 TRM
d) NRM
1
KAM1-4.2B11
150
300
490
560
E
N
Down
NRM = 0.68 A.m²/kg
Rejected
1
TRM

Figure 6

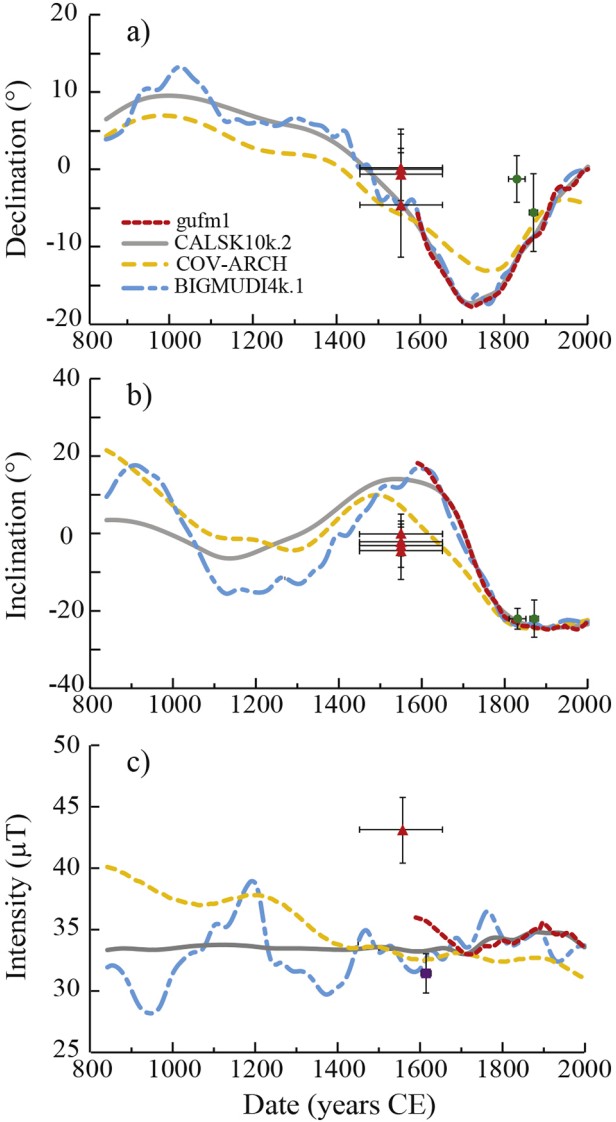
a)
b)
c)
Declination (°)
Inclination (°)
Intensity (μT)
Date (years CE)
gufm1
CALSK10k.2
COV-ARCH
BIGMUDI4k.1

Figure 7

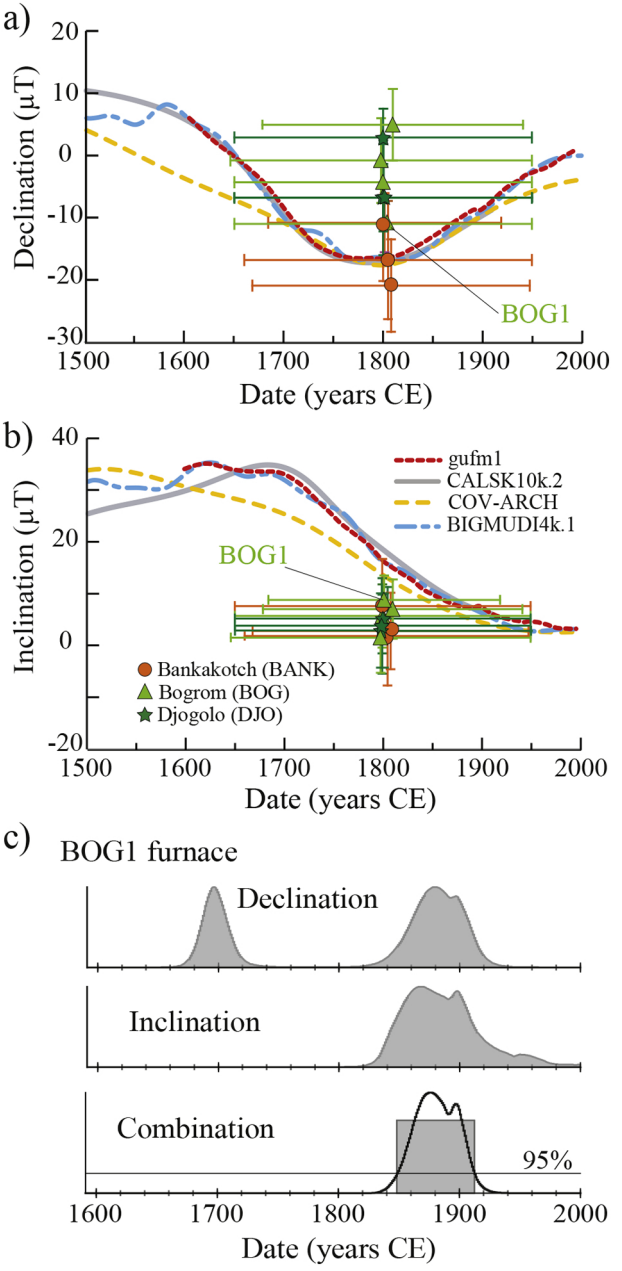
a)
Declination (μT)
20
10
0
-10
-20
-30
BOG1
1500
1600
1700
1800
1900
2000
Date (years CE)
b)
Inclination (μT)
40
20
0
-20
gufm1
CALSK10k.2
COV-ARCH
BIGMUDI4k.1
BOG1
Bankakotch (BANK)
Bogrom (BOG)
Djogolo (DJO)
1500
1600
1700
1800
1900
2000
Date (years CE)
c)
BOG1 furnace
Declination
Inclination
Combination
95%
1600
1700
1800
1900
2000
Date (years CE)

Figure 8